RSC Advances

PAPER

View Article Online
View Journal | View Issue

Cite this: *RSC Adv.*, 2025, **15**, 4356

Synergistic activation of peroxymonosulfate by highly dispersed iron-based sulfur–nitrogen co-doped porous carbon for bisphenol a removal: mechanistic insights and selective oxidation†

Yu Sun, Chuning Zhang, Yan Jia, * Yalei Zhang and Jianwei Fan

Efficient and pervasive solutions are urgently needed to mitigate pollution from emerging contaminants in aquatic environments. Activation of peroxymonosulfate (PMS) is commonly employed to remove refractory organic pollutants from water. Herein, we synthesized sulfur–nitrogen co-doped porous carbon materials loaded with highly dispersed iron species (FeSNC) using template-assisted and ligand site construction methods. The uniform doping of N, S, and Fe in the carbon substrate, along with their synergistic effects, significantly enhanced catalytic activity by creating a high degree of defects in the catalyst (I_D/I_G = 1.47). This enhancement facilitated efficient removal of BPA, achieving an apparent rate constant of up to 2.83 min^{-1}, which was 30 times higher than that of SNC and 6 times higher than that of FeNC. The FeSNC/PMS system demonstrated robust catalytic stability across the pH 3–9 range, and showed minimal sensitivity to environmental factors like the aqueous matrix, with low iron ion dissolution (<0.01 mg L^{-1}) and certain reusability. Mechanistic investigations employing quenching experiments, EPR tests, probe experiments, and electrochemical tests elucidated that the system catalyzed the degradation of BPA *via* two non-radical pathways: high-valent iron oxidation and singlet oxygen pathways. Additionally, the system further exhibits selective degradation of electron-rich organics (*e.g.*, 4-chlorophenol, sulfamethoxazole, ofloxacin, *etc.*).

Received 12th December 2024
Accepted 23rd January 2025

DOI: 10.1039/d4ra08729a

rsc.li/rsc-advances

1 Introduction

With the process of industrialization and the development of the chemical industry, contaminants of emerging concern (CECs), also known as "emerging contaminants (ECs)", are constantly emerging in the atmosphere, soil, water, and other environmental mediums.[1] Due to their structural stability and solubility, CECs that enter aquatic environments are recalcitrant (difficult to degrade naturally) and persist through wastewater treatment. This persistence allows CECs to bioaccumulate in humans and animals through consumption of contaminated food and water, posing a serious threat to human health and the ecological balance.[2–4] In the treatment of refractory organic pollutants in water column, advanced oxidation technologies (AOPs) have outstanding advantages over other treatments due to their fast reaction speed and strong oxidizing ability, which can efficiently mineralize various types of refractory organic pollutants into CO_2 and H_2O and remove them completely.[5,6] Currently, AOPs with more industrial applications include Fenton oxidation,[7] ozone oxidation,[8] supercritical oxidation[9] and wet oxidation.[10] Catalytic oxidation based on the peroxymonosulfate (PMS) system stands out due to its high application value and research significance. This system offers several advantages, including high oxidation potential, a wide range of adapted pH, and safe storage and transportation of the oxidant.[11,12]

Beyond traditional methods like heat, radiation, and alkali activation, employing non-metal catalysts (graphene, carbon nanotubes, graphitized nano-diamonds, biochar) avoids heavy metal contamination of aquatic environments compared to conventional heavy metal catalysts. However, the catalytic degradation of pollutants in water using pure carbon materials for peroxymonosulfate activation often suffers from slow degradation rate and catalyst failure due to oxidation by its own catalytic reactive oxygen species (ROS).[13] Metal doping is a well-established strategy to improve the catalytic activity of carbon materials. In recent years, metal–carbon catalysts with desirable physicochemical properties have been synthesized using a variety of transition metals, such as iron,[14,15] cobalt,[16] copper,[17] manganese,[18] and nickel,[9] as additives. However, transition metals, transition metal alloys and their oxide materials often have problems in the catalytic degradation of pollutants by

State Key Laboratory of Pollution Control and Resources Reuse, College of Environmental Science and Engineering, Shanghai Institute of Pollution Control and Ecological Security, Tongji University, Shanghai 200092, P.R. China. E-mail: jiay@tongji.edu.cn

† Electronic supplementary information (ESI) available. See DOI: https://doi.org/10.1039/d4ra08729a

peroxymonosulfate, such as the low number of exposed metal sites in loaded metal catalysts due to the natural aggregation tendency of the metal sites, and the pollution of aqueous environments by leaching metals.[19] Compared with other transition metals, iron is a particularly attractive metal for catalyst development due to its abundance and environmental friendliness, making the enhancement of catalytic performance of iron-based catalysts a popular research topic.[20,21]

In the past few years, a large number of studies have been conducted on highly dispersed or even dispersed to the atomic level iron–nitrogen–carbon (Fe–N–C) catalysts, which have been shown to possess both the uniform and efficient activity of homogeneous catalytic systems and the easy separation and structurally stable and recyclable characteristics of heterogeneous catalytic systems, which can efficiently activate peroxides (persulfate, hydrogen peroxide, periodate, *etc.*) for the degradation of organic compounds.[20,22,23] The introduced heteroatoms (N, P, S, B) can influence the formation of active centers and structural species of iron-based materials to enhance the adsorption and activation effects of the materials.[24,25] Baitao Li *et al.*[26] used a metallic organic framework derived carbon framework co-doped by Fe, S, N tri-elements as an alternative electrocatalyst to the conventional Pt/C cathode catalyst, and the performance of microbial fuel cell was improved by enhancing the kinetics of cathodic oxygen reduction reaction. Lei Jiao *et al.*[27] synthesized atomically dispersed Fe atoms on hierarchically S/N co-doped porous carbon (FeSNC) using a template-assisted method with unsymmetrically coordinated Fe–N_3S_1 as the active sites, which improves the peroxidase-like activity and achieves a sensitive detection of organophosphorus pesticides. Heng Liu *et al.*[28] has explored the role of sulfur functionalities in regulating the electron distribution of single-atomic Fe sites by the construction of single-atomic Fe–N_4 sites with sulfur functionalities (FeSNC) using sulfur-containing molecules with different molecular structures. It is shown that the sulfur functionalities of thiophene S and oxidized S both possess the electron-donating properties, which can regulate the electronic configurations of Fe–N_4 site, resulting the weakened adsorption of ORR intermediates and thus accelerating the kinetics of the ORR process. Based on this, it is reasonable to assume that sulfur- and nitrogen co-doped iron-based catalysts have good potential for enhancing Fenton-like catalysis.

Here, sulfur–nitrogen co-doped porous carbon materials (FeSNC) loaded with highly dispersed iron species, as well as contrasting materials, were synthesized using template-assisted and ligand site-constructed methods for activating PMS for pollutant removal in the aqueous phase. Bisphenol A (BPA), a typical endocrine disrupting compounds (EDCs), was used as a target pollutant to test the catalytic performance of the catalysts for PMS. The morphology, specific surface area and elemental valence states of the synthesized catalysts were characterized. Due to the co-doping of sulfur and nitrogen atoms and the synergistic effect of iron sites on each other, FeSNC showed the best results in activating PMS for the removal of BPA, with an apparent degradation rate constant of 2.83 min^{-1}. The catalytic effect was highly stable in the range of pH 3–9 and was almost independent of the environmental factors, such as ions in the aqueous phase and quenching effect of organics. FeSNC/PMS system had extremely low iron ion dissolution (<0.01 mg L^{-1}) and was reusable. In addition, the FeSNC/PMS system was proposed to catalyze the degradation of BPA *via* two non-radical pathways (high-valent iron oxidation pathway and single-linear oxygen pathway) through quenching studies, probe experiments, and electrochemical tests. The FeSNC also exhibited degradation selectivity for electron-rich organics (*e.g.*, 4-chlorophenol, sulfamethoxazole, ofloxacin, *etc.*).

2 Experimental

2.1 Preparation of FeSNC

SiO_2 spheres enriched with surface groups were prepared as hard templates by the typical Stöber method.[29] FeSNC, a controllable sulphur–nitrogen co-doped carbon material with hyperdispersed iron active sites, was synthesized by the hard template method using $Fe(NO_3)_3 \cdot 9H_2O$ as the metal precursor and 1-allylthiourea as the sole sulphur, nitrogen and carbon source. As detailed in Fig. S1,† quantitative SiO_2 spheres, 1-allylthiourea and $Fe(NO_3)_3 \cdot 9H_2O$ were ultrasonicated in ultrapure water and mixed and stirred at 70 °C for 12 h. The mixture was dried by slow evaporation in an oven at 60 °C, and the reddish-brown solid powder obtained was pyrolyzed under argon atmosphere in a tube furnace at 700 °C, 900 °C, and 1100 °C for 3 h at a heating rate of 5 °C min^{-1}, respectively. The black powder obtained was first placed in 50 °C solution of 5.0 M NaOH and stirred for 6 h to remove the hard template spheres, followed by washing with ultrapure water twice and centrifugation for collection, and then passed through 1.0 M H_2SO_4 solution and stirred for 1 h to remove the possible large metal particles. The products were vacuum dried at 60 °C overnight to obtain FeSNC, named FeSNC-700, FeSNC-900 and FeSNC-1100 depending on the pyrolysis temperature. As a comparison, sulphur–nitrogen–carbon (SNC) and iron–nitrogen–carbon (FeNC) catalysts were also prepared.

In addition, the details about the reagents and chemicals, and the characterizations of catalysts are provided in ESI (Texts S1 and S2).†

2.2 Catalytic activity test

The high efficiency of the catalyst in activating PMS for degradation of organic pollutants was demonstrated with bisphenol A (BPA), rhodamine B (RhB), 4-chlorophenol (4-CP), sulfamethoxazole (SMX), nitrobenzene (NB), benzoic acid (BA), 4-nitrophenol (4-NP), and ofloxacin (OFL), as the target pollutants. The degradation experiments were carried out in a beaker. A quantitative amount of catalyst was added to 25 mL of BPA solution (20 mg L^{-1}), sonicated for 30 s to make full dispersion, and stirred for 10 min at 300 rpm to reach adsorption equilibrium, after which a quantitative amount of PMS was added to initiate the catalytic reaction. 1.0 mL of the solution was removed at the set time interval, and the reaction was immediately terminated by filtration through a 0.22 μm cellulose acetate membrane into a solution containing 20 μL $Na_2S_2O_3$ (0.5

M), and the concentration of the filtrate was analyzed by HPLC. The influences of various factors, including different pyrolysis temperatures (700–1100 °C), catalyst dosages (0–0.2 g L^{-1}), PMS dosages (0.1–2 mM), initial pH of solutions,[3–9] coexisting inorganic anions and organic pollutant species, were investigated. The catalytic stability of FeSNC was also evaluated through cycling tests. Reactive oxygen species quenching experiments and probe experiments were used to explore the reaction mechanism. Deionized water was used for all experiments. In exploring the effect of pH on the system, at pH 3.0, the pH was adjusted by manually adding perchloric acid; when the experiments were conducted at pH 5.0 and above, the pH dropped significantly due to the decomposition of PMS, thus a mixture of acetic acid–sodium acetate solution and boric acid–sodium borate solution was used as a buffer to keep the pH constant during the reaction.

2.3 Analytical methods

The concentrations of bisphenol A (BPA), 4-chlorophenol (4-CP), sulfamethoxazole (SMX), nitrobenzene (NB), benzoic acid (BA), and ofloxacin (OFL) were determined by high performance liquid chromatography (HPLC, Agilent HPLC 1200) with a UV lamp using an Agilent 5 TC-C18 column (150 × 4.6 mm, 5 μm). The specific detection methods for different pollutants are shown in Table S1.† The concentration of rhodamine B (RhB) and 4-nitrophenol (4-NP) were measured by UV-vis spectrophotometer (UV765) at the maximum absorption wavelengths of 554 and 317 nm, respectively. The total organic carbon (TOC) was identified by a TOC analyzer (Vario TOC, Thermo Fisher Scientific). Fe leaching of catalysts during the reactions was also measured by inductively coupled plasma optical emission spectrometer (ICP-OES, Agilent 5110). In quenching experiments, EtOH, MeOH, TBA, FFA, p-BQ, KSCN and PMSO were selected as quenching agents to determine the active species in the system. Additionally, electron paramagnetic resonance (EPR) measurement was performed on a Bruker EMXplus-6/1 spectrometer, as detailed in Text S3.† Electrochemical measurements were performed at the CHI 660D electrochemical workstation, as detailed in Text S4.†

3 Results and discussion

3.1 Properties of the catalysts

The surface morphology and elemental distribution of FeSNC were measured by SEM and SEM-mapping. Fig. 1(c) and (d) shows a hard template of SiO_2 nanospheres with an average diameter of about 150 nm prepared by the modified stöber method, and the void size of FeSNC is comparable to the size of SiO_2 nanospheres. After removal of the SiO_2 templates, FeSNC showed an irregular skeletal structure composed of porous carbon with the presence of graphitized structure (Fig. 1(a) and (b)), which gave the catalyst a larger specific surface area and more exposed active sites for promoting mass transfer. No obvious particles were observed on the surface of FeSNC, indicating that the loaded iron elements were highly dispersed in the carrier. Combined with the elemental distribution images in Fig. 1(e), it reveals that the elements C, N, Fe, and S are highly and uniformly dispersed on the catalyst surface.

The crystal structures of the catalysts were obtained using XRD (Fig. 2(a)). The SNC, FeNC and FeSNC catalysts showed two broad and weak diffraction peaks near 26.3° and 44.3°, which can be attributed to the characteristic derivation peaks on the (002) and (101) facets of graphitic carbon (JCPDS No. 41-1487). It indicates that the graphitic carbon is structurally disordered and defective.[30,31] It is noteworthy that no characteristic metal peaks were observed in the XRD plots, further demonstrating the absence of metal-related particles and that the synthesized iron species are highly dispersed on the surface of the carbon material.

Raman is commonly used to evaluate the degree of defects in carbon materials. As shown in Fig. 2(c), the D band (carbon layer defects/disorder) and the G band (crystalline graphitic carbon) are two peaks in the sample, located at 1350 cm^{-1} and 1580 cm^{-1}, respectively, and the degree of defects in the carbon material was assessed by fitting the D and G peaks to obtain the I_D/I_G intensity ratio and comparing the degree of graphitization.[32] The I_D/I_G value of FeSNC is 1.47, and the Raman spectrum shows a high D band, indicating that the surface of FeSNC is highly disordered with many lattice defects. The high degree of defects in the material can be attributed to Fe reduction

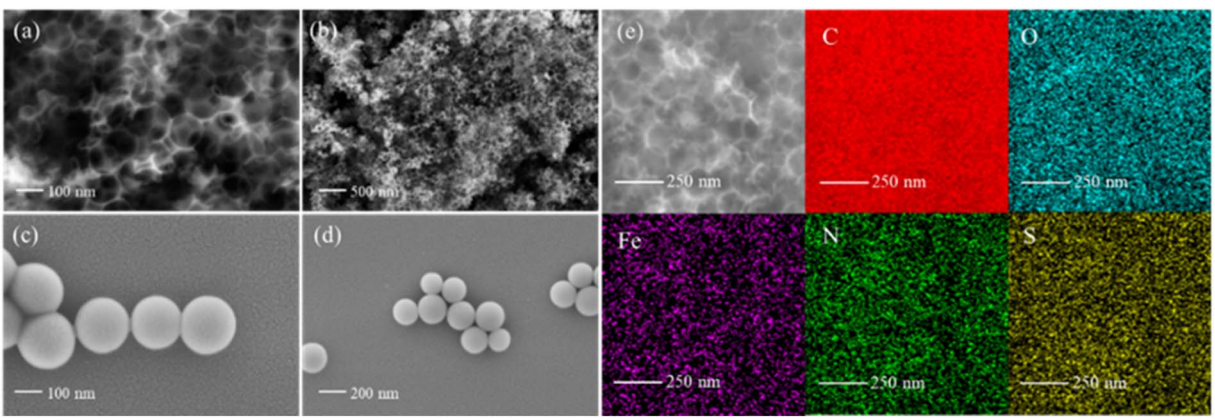

Fig. 1 SEM images of (a and b) FeSNC and (c and d) SiO_2; (e) elemental distribution of FeSNC.

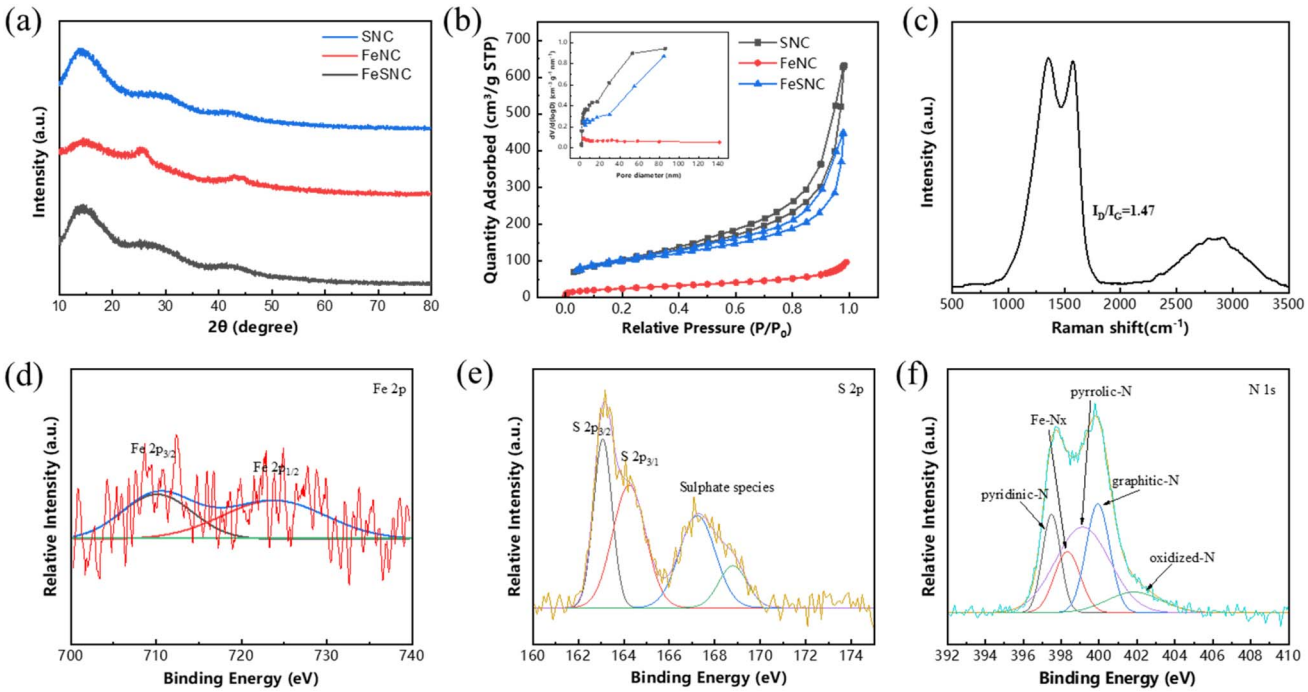

Fig. 2 (a) XRD pattern of SNC, FeNC and FeSNC; (b) N_2 adsorption–desorption isotherms of SNC, FeNC and FeSNC; (c) Raman spectra of FeSNC; high-resolution XPS spectrum of (d) Fe 2p, (e) S 2p and (f) N 1s of FeSNC.

during pyrolysis, gasification of allyl thiourea and co-doping of Fe, N and S.[29,33–35]

The chemical elemental composition and elemental valence states of the FeSNC catalyst surface were probed by XPS. As shown in Fig. S2,† the full spectrum of XPS indicates that the material is mainly composed of five elements, C, N, O, S and Fe. According to Table S2,† the content of N and S elements on the catalyst surface reached 6.84 at% and 1.12 at%, respectively, indicating that both S and N elements were dispersed on the surface of the carbon material, and the synthesis process successfully introduced S doping. The deconvolution of the high-resolution Fe 2p profile of FeSNC (Fig. 2(d)) splits into two peaks located in the Fe $2p_{3/2}$ orbitals around 709.98 eV and the Fe $2p_{1/2}$ orbitals around 724.3 eV, indicating that there is no or a small amount of Fe–Fe bonding in FeSNC, *i.e.*, there are no metal monolithic nanoparticles present in the synthesized catalyst sheet, and highly dispersed iron sites are mainly present in the oxidation state.[36,37] Fig. 2(e) shows the high-resolution S 2p profile of FeSNC with two main peaks located around 163.3 and 164.6 eV, corresponding to the S $2p_{3/2}$ and S $2p_{1/2}$ peaks of the thiophene-S species (C–S–C) in the sample, and small peaks were also observed around 167.6 eV and 168.8 eV, corresponding to the oxide S species.[38] Thiophene-S and oxide-S act as electron donors and absorbers, respectively, on the surface of carbon materials and can influence the electron distribution effect on the carbon surface.[39] The high-resolution N 1s spectrum of FeSNC can be deconvoluted into five peaks near 397.6 eV, 398.5 eV, 399.5 eV, and 402.4 eV (Fig. 2(f)), which corresponds to the pyridine-N, Fe–N_x, pyrrole-N, graphite-N, and oxidized-N.[40] The presence of Fe–N_x once again demonstrates that the iron on the catalyst surface is anchored by nitrogen, avoiding agglomeration and presenting a highly dispersed state.[41] A significant amount of literature reports that high Fe–N_x and graphite-N contents in materials favor PMS catalysis.[42–44]

The pore structures of SNC, FeNC and FeSNC were characterized by N_2 adsorption–desorption method, and the N_2 adsorption–desorption isotherms and pore size distribution curves of the three materials are shown in Fig. 2(b). As shown, the shapes of the N_2 adsorption–desorption isotherms of SNC and FeSNC are similar, and all of them present type IV adsorption isotherms of microporous/mesoporous materials with typical H3 hysteresis loops, which confirm the existence of the microporous/mesoporous structure. The adsorption–desorption isotherm type of FeNC material belongs to type II of the IUPAC classification, and the hysteresis loop belongs to type H3. Comparing the corresponding specific surface area, pore volume and pore size of the three materials based on the results of the nitrogen adsorption–desorption method (Table S3†). The specific surface areas of FeNC, SNC and FeSNC were 90.1 $m^2 g^{-1}$ and 360.7 $m^2 g^{-1}$ and 349.1 $m^2 g^{-1}$, respectively, suggesting that the gasification of allyl thiourea introduced by S doping increases the pore structure of the carriers drastically, while the subsequent loading of iron clogs a part of the pores, leading to a decrease in the specific surface area.

3.2 Catalytic performance evaluation

To evaluate the catalytic activity of the synthesized FeSNC catalysts, BPA was selected as a model pollutant and the performance of SNC, FeNC and FeSNC activated PMS for the degradation of BPA was investigated (Fig. 3). The extent of BPA mass concentration reduction, which was almost absent when

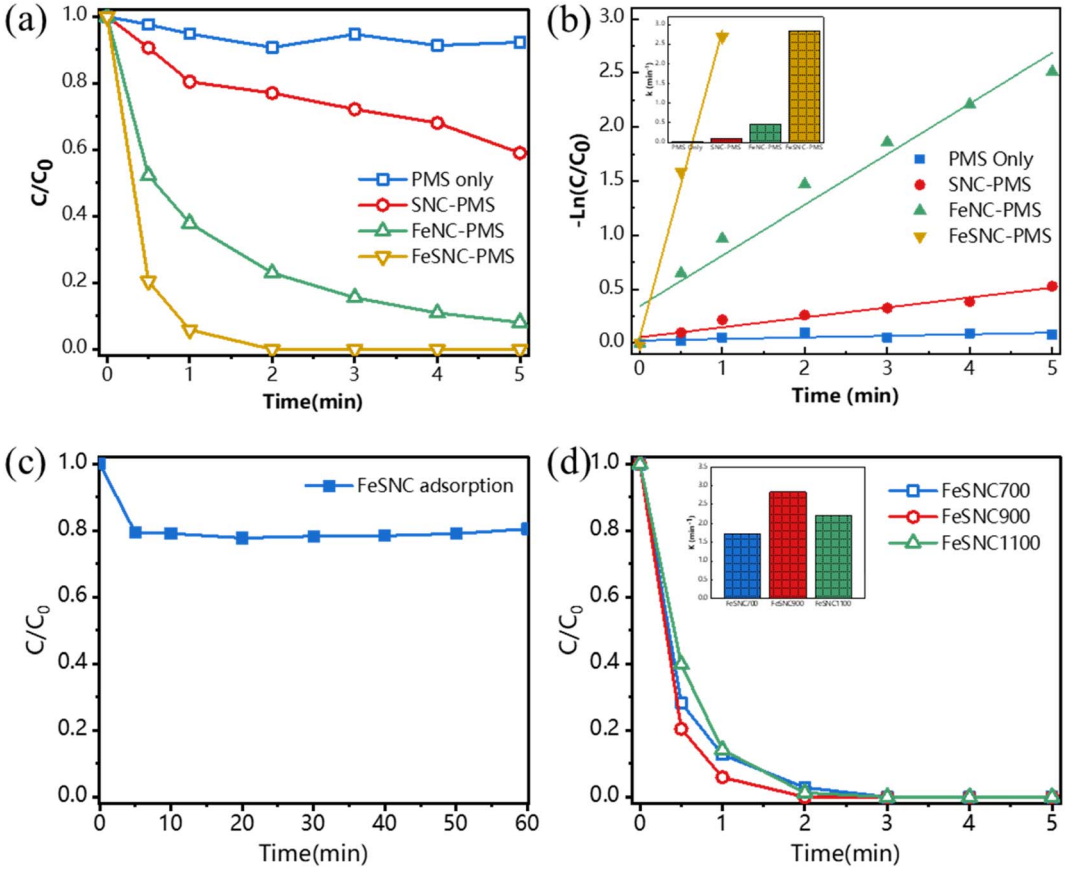

Fig. 3 (a) Degradation kinetic curves and (b) pseudo-first-order kinetic fitting of BPA by different catalytic systems; (c) degradation kinetic curve of BPA adsorption by FeSNC; (d) degradation kinetic curves and apparent rate constant (k_{obs}) of BPA by FeSNC prepared at different pyrolysis temperatures. Experimental conditions: $[BPA]_0 = 20$ mg L^{-1}, $[PMS]_0 = 1$ mM, $[catalyst]_0 = 0.10$ g L^{-1}, initial pH 4.2.

only PMS was used, suggests the limited role of PMS self-activation in generating reactive radicals.[45,46] The adsorption of FeSNC on BPA can approach the adsorption equilibrium in about 5 min (Fig. 3(c)), so we chose to stir the catalysts for 15 min to reach the adsorption equilibrium before adding PMS to initiate the catalytic oxidation reaction. The BPA degradation rates of SNC-PMS, FeNC-PMS and FeSNC-PMS systems reached 41%, 91% and 100% in 5 min, respectively, with the FeSNC-PMS system amazingly reaching 100% degradation in 3 min. The results show that both sulfur modification and Fe loading of the nitrogen–carbon materials result in stronger activation of PMS. Based on the literature research, FeSNC was compared with other reported PMS catalysts, and the results are shown in Table S4,† which shows that the catalytic activity of FeSNC synthesized in this study is very high, and it can activate PMS to degrade 20 mg L^{-1} of BPA in 3 min, and the reaction time is significantly shorter than most of the reported typical catalysts, including metal-based catalysts, under similar reaction conditions, metal-based catalysts, pure carbon-based catalysts, and metal–carbon based catalysts.

Calcination temperature also has an effect on the catalytic activity of the synthesized catalysts, so FeSNC at different calcination temperatures were synthesized to discuss the calcination temperature that achieves the optimal catalytic activity. As shown in Fig. 3(d), the BPA degradation rate increased when the calcination temperature was increased from 700 °C to 900 °C, and then decreased to a certain degree when the calcination temperature was further increased to 1100 °C. This may be due to the reconstruction of the carbon substrate in the reduction process of iron species, which leads to a change in the defect density of the synthesized catalysts, including vacancies, edges, and topologic defects.[47,48] FeSNC900 synthesized at 900 °C fully utilized the PMS, which had the best degradation effect of BPA. Therefore, all the subsequent experimental subjects were FeSNC900 synthesized at 900 °C, which was denoted as FeSNC for the sake of simplicity.

In addition, the actual metal contents of FeSNC and FeNC measured by inductively coupled plasma emission spectroscopy are shown in Table S5,† in which FeSNC contains 0.64 wt% of elemental iron 0.133 times more than that of FeNC, but the apparent degradation reaction rate constant k_{obs} value of FeSNC reaches 2.83 min^{-1}, while the comparison material FeNC is only 0.64 min^{-1}, which reflects the low metal leaching risk and high metal site utilization of FeSNC catalyst.

3.3 Experimental conditions optimization

In the PMS activation system, the catalyst FeSNC dosage affects the BPA degradation efficiency. The effect of FeSNC dosing on BPA degradation was explored by varying the FeSNC dosage (0,

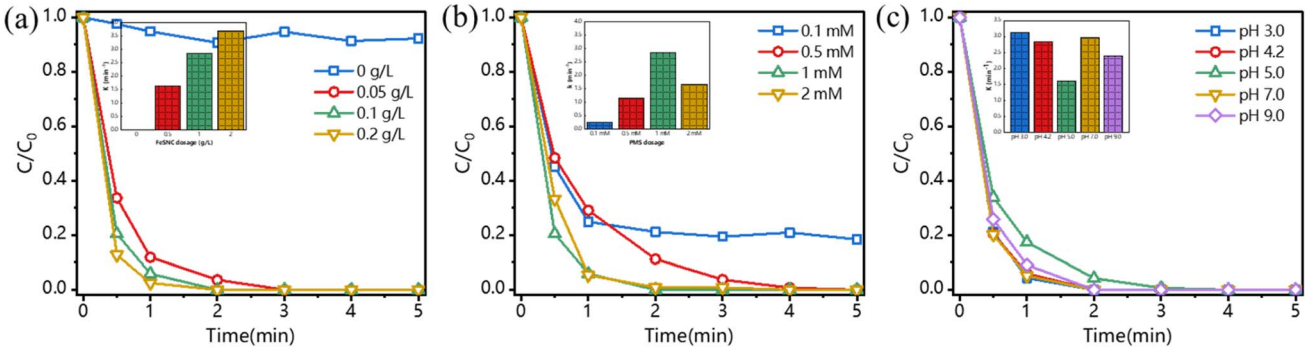

Fig. 4 Kinetic curves of BPA degradation and apparent rate constant (k_{obs}) by FeSNC-PMS system with (a) different catalyst dosage, (b) different PMS concentration and (c) different initial pH. Experimental conditions: $[BPA]_0 = 20$ mg L^{-1}, $[PMS]_0 = 1$ mM, $[catalyst]_0 = 0.10$ g L^{-1}, initial pH 4.2.

0.05 g L^{-1}, 0.10 g L^{-1}, and 0.20 g L^{-1}), and the results are shown in Fig. 4(a). It shows that the BPA degradation rate increased with the increase of FeSNC dosage. When the FeSNC dosage was 0.05 g L^{-1}, 0.10 g L^{-1} and 0.20 g L^{-1}, BPA was completely eliminated within 3 min. The apparent rate constant k_{obs} for BPA degradation increased from 1.6 min^{-1} to 3.6 min^{-1} when the FeSNC dosage was increased from 0.05 g L^{-1} to 0.20 g L^{-1}. With the increase of FeSNC dosage, the active sites in the reaction system FeSNC-PMS were increased, which allowed the BPA to be degraded more rapidly, but in order to avoid the ROS elimination reaction that might be caused by too much catalyst, the FeSNC dosage of 0.10 g L^{-1} was selected as the condition for the reaction to be carried out in order to consider the economic efficiency.

The concentration of PMS also affects the efficiency of BPA degradation in the FeSNC-PMS system, so the degradation of BPA was explored at PMS concentrations of 0.1 mM, 0.5 mM, 1 mM, and 2 mM. As shown in Fig. 4(b), when the concentration of PMS was increased from 0.1 mM to 0.5 mM, the degradation efficiency of BPA increased from 80% to 100% within 5 min. When the PMS concentration continued to increase to 2 mM, BPA was completely degraded within 5 min. However, the apparent rate constant k_{obs} decreased significantly when the PMS concentration was increased from 1 mM to 2 mM. This might be attributed to the fact that the presence of excess PMS has a depleting effect on ROS, thus inhibiting the degradation of the reaction substrate BPA.[49] In order to avoid the inhibitory effect of excess PMS, the PMS concentration of 1 mM was chosen for subsequent experimental investigations.

The pH of the reaction affects the surface properties of the catalyst and the ionization state of the pollutant, so the effect of pH changes from 3.0 to 9.0 on the degradation of BPA by the FeSNC-PMS system was explored. The results, as shown in Fig. 4(c), showed that the degradation rate of BPA by FeSNC-PMS system reached more than 99% within 3 min, which proved that the degradation effect of FeSNC-PMS system was very stable and efficient in the interval of pH = 3 to pH = 9. The main reasons for the influence of pH on the catalytic oxidation process are as follows: (i) the charge of the pollutant, catalyst, and oxidant; (ii) the existing form of the oxidant; and (iii) the mutual interaction and type of transformation of reaction groups at different pH values.[50] Thus, the main ROS generated in the FeSNC-PMS system are more likely to be non-radicals that are less susceptible to pH interference than the traditional radical degradation pathway that is strongly influenced by pH.

3.4 Reaction mechanism

Active species including radicals and oxygen-contained species were scrutinized throughout the FeSNC-PMS system using a scavenging trial (Fig. 5(a)). EtOH, MeOH and TBA were quenchers of sulfate radicals ($SO_4^{\bullet-}$) and hydroxyl radicals ($^{\bullet}OH$) respectively, *p*-benzoquinone (p-BQ) was an inhibitor of super oxygen ($O_2^{\bullet-}$) and singlet oxygen ($^1O_2$) was inhibited by FFA.[51–53] The degradation rate of BPA was consistent when EtOH, MeOH and *p*-benzoquinone were added, respectively, with a slight decrease relative to the blank, and the degradation efficiency could still reach more than 99% within 2 min, indicating that the effects of free radicals in the FeSNC-PMS system, such as $SO_4^{\bullet-}$, $^{\bullet}OH$ and $O_2^{\bullet-}$, were negligible. Moreover, the quenching results did not change significantly when adjusting the dosage of MeOH (Fig. 5(b)). The FFA dosing with low molar ratio (FFA/PMS = 10) had some inhibitory effect on the degradation of BPA, and when the molar ratio was increased to FFA/PMS = 1000 and FFA/PMS = 100, the oxidation reaction was inhibited to a similar extent, and the degradation rate reached 90% within 5 min, which proved that $^1O_2$ was produced in the activated PMS system, but other ROS still existed to play a major role in the efficient degradation of the BPA reaction (Fig. 5(c)). KSCN, as a masking agent for iron sites, was added and the reaction was significantly inhibited with almost no degradation of BPA, suggesting that the active site of the catalyst is related to the iron site.[54] Both MeOH ($k_{SO_4^{\bullet-}}$=(0.2 − 2.5) × 10^7 M^{-1} s^{-1}; $k_{^{\bullet}OH}$=(0.78 − 1.0) × 10^9 M^{-1} s^{-1}) and EtOH ($k_{SO_4^{\bullet-}}$ = (1.6 − 7.7) × 10^7 M^{-1} s^{-1}; $k_{^{\bullet}OH}$ = (1.6 − 2.2) × 10^9 M^{-1} s^{-1}) were reported to react simultaneously with $SO_4^{\bullet-}$ and $^{\bullet}OH$, whereas the reaction rate of TBA ($k_{SO_4^{\bullet-}}$ = (4.0 − 9.1) × 10^5 M^{-1} s^{-1}; $k_{^{\bullet}OH}$ = (3.8 − 7.6) × 10^8 M^{-1} s^{-1}) with $^{\bullet}OH$ reacts at a rate several orders of magnitude higher than that with $SO_4^{\bullet-}$.[55,56] Theoretically, the inhibition effect of adding EtOH and MeOH on the free radical reaction should be higher than that of adding TBA.[57] However, the degradation rate in the experimental results with the addition of TBA was reduced compared to the reaction rate in both

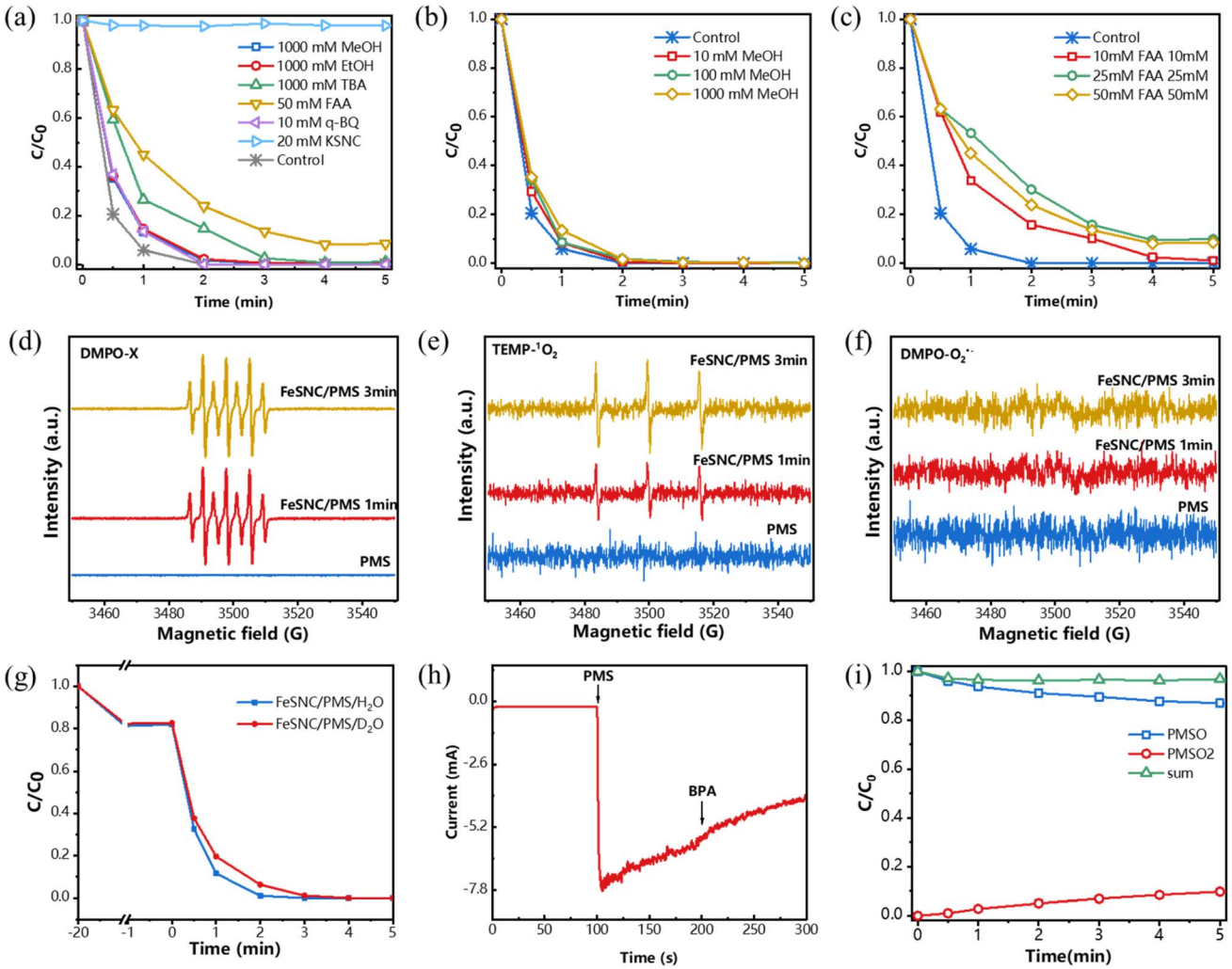

Fig. 5 (a–c) Impact of scavengers on BPA degradation in the FeSNC/PMS system; EPR analysis for DMPO-X (d), $^1O_2$ (e), and $O_2^{\bullet-}$ (f) detection of FeSNC/PMS system; (g) BPA degradation efficiency in different solvents; (h) amperometric *I*–*t* curves upon the addition of PMS and BPA; (i) PMSO loss and $PMSO_2$ production in the FeSNC/PMS system.

the blank control and the EtOH and MeOH groups, and the degradation rate was less than 85% at 2 min of reaction. The contradictory experimental phenomenon may be attributed to the fact that the addition of TBA changed the solution and catalyst surface properties, resulting in catalyst agglomeration.

EPR tests further identified the ROS generated in the FeSNC/PMS system by capturing the free radicals and $^1O_2$ generated in the FeSNC/PMS system with DMPO and TEMP in water or methanol solvent, respectively.[58] As shown in Fig. 5(d–f), no EPR intensity signals were detected in the presence of PMS alone. And no signal peaks of DMPO-$^{\bullet}$OH and DMPO-$SO_4^{\bullet-}$ were detected in the reaction solution of the FeSNC/PMS system, which indicates that $SO_4^{\bullet-}$ and $^{\bullet}$OH radicals are hardly generated in the FeSNC/PMS system; meanwhile, a seven-line spectrum representing the intensity ratio of DMPOX in the ratio of 1 : 2 : 1 : 2 : 1 : 2 : 1 was observed to be present in the system (a_N = 7.4 G, a_H = 3.9 G). DMPOX is an oxidation product resulting from the oxidation of DMPO, and the presence of DMPOX implies the presence of strong oxidizing substances that can be oxidized at high rates in the FeSNC/PMS system.[30,59] TEMP-trapping experiments in the FeSNC/PMS system observed typical 1 : 1 : 1 triplet peak indexing to TEMP-$^1O_2$ (a_N = 16.9 G), and the intensity increased with the reaction time, which proved the presence and accumulation of $^1O_2$.[60] Combined with the results of the quenching experiments, $^1O_2$ is not the main ROS in the FeSNC/PMS system, and in order to further explore the strongly oxidizing species that produce DMPOX, $O_2^{\bullet-}$ were detected in the FeSNC/PMS/DMPO/MeOH system. As shown in Fig. 5(f), no significant EPR signals for DMPO-$O_2^{\bullet-}$ were detected, indicating that $O_2^{\bullet-}$ was hardly present in the FeSNC/PMS system, whereas $O_2^{\bullet-}$ was reported as a generated $^1O_2$ intermediate species in the relevant literature, and thus the presence of $^1O_2$ needs to be further explored.[61]

$^1O_2$ has been reported to exist about ten times longer in deuterium oxide (D_2O) (20–30 μs) than in H_2O (2 μs), and taking D_2O as a medium reaction will be faster than H_2O medium if a large amount of $^1O_2$ is generated in the reaction system.[49] However, the results in Fig. 5(g) show that the degradation rate

becomes slower in the D_2O system relative to the H_2O system, which confirms that $^1O_2$ is not generated in large quantities in the activated PMS system, and proves that the strong oxidizing substance for oxidative generation of DPMOX is not $^1O_2$.

Electron transfer is also one of the pathways for pollutant degradation *via* activation of persulfate by carbon-based catalysts, in which the pollutants are directly oxidized by providing electrons to the oxidant with the catalyst as a bridge, resulting in the immediate oxidation of the pollutant without the generation of ROS during the reaction.[62] The chronoamperometry tests method in electrochemistry has been used to verify the existence of a mediated electron transfer mechanism in the FeSNC/PMS system. As shown in Fig. 5(h), a sudden change in current occurred after the addition of PMS at 100 s, indicating that the electron transfer between the catalyst surface and PMS occurred; whereas, the current magnitude did not change with the addition of BPA at 200 s, suggesting that the electron transfer process from BPA to PMS with FeSNC as the bridge did not occur. This indicates that the electron transfer in the FeSNC/PMS system occurs during the reaction between PMS and FeSNC to generate ROS, and the surface electron transfer pathway is not the sulfate activation pathway in the FeSNC/PMS system.

In addition, the Fe sites in the catalyst can form high-valent iron–oxo complexes ($\equiv Fe^{IV}=O$ and $\equiv Fe^{V}=O$) on reaction with PMS, and similar to the non-radical reaction pathway, this reactive intermediate can oxidize pollutant molecules efficiently and is unaffected by other organics quenchers, such as ethanol, methanol, and so on.[63] The transformation efficiency from methyl phenyl sulfoxide (PMSO) to the corresponding sulfone ($PMSO_2$) has been used to indicate the contribution of high-valent metal species in the AOPs.[64] As shown in Fig. 5(i), the content of PMSO decreased to 82.4% after 10 min of reaction in the FeSNC/PMS system, while the generation of $PMSO_2$ was 14.6%, indicating that the high-valent iron–oxo complexes played a significant role in the FeSNC/PMS system. In addition, the formation of high-valent iron–oxo complexes leads to a change in the binding energy of Fe, which is shifted in the direction of high binding energy compared to that of Fe in the low-valent state. Comparing the high-resolution XPS patterns of Fe before and after the reaction (Fig. 2(d) and S5(b)†), the shift of the characteristic peaks of Fe element towards higher binding energy also confirms the generation of high-valent iron–oxo complexes. On this basis, it can be assumed that the DMPOX detected in the FeSNC/PMS/DMPO/H_2O system was generated by the rapid oxidation of the high-valent iron–oxo complexes.

In summary, the reaction mechanism of FeSNC degradation of BPA by activation of PMS is proposed as shown in Fig. 6. In detail, PMS was first adsorbed onto the FeSNC surface and then activated to generate ROS, which could react with BPA adsorbed onto the FeSNC surface and in solution for oxidation. Activation of PMS by FeSNC occurred mainly through two non-radical pathways, high-valent metal species and singlet oxygen ($^1O_2$). For the singlet oxygen pathway, FeSNC is not recombined to generate $^1O_2$ *via* the decomposition of PMS into the intermediate $O_2^{\cdot-}$ after oxidation in contact with the sites, as the intermediate $O_2^{\cdot-}$ was not detected by EPR tests.[31,65,66] Thus, $^1O_2$ can be generated mediated by the transfer of electrons from M–N–C and M–O–C bonds and activation of the carbon layer to form peroxides, as hypothesized by existing studies.[67] For the high-valent metal oxidation pathway, the Fe–N_x active site in

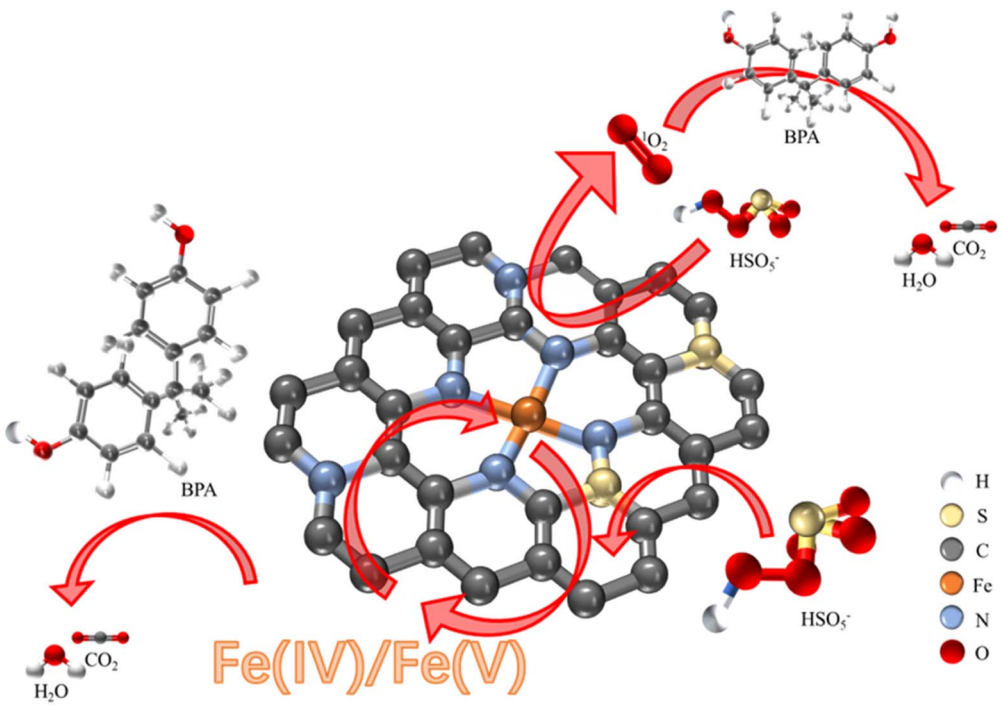

Fig. 6 Possible catalytic mechanism of BPA degradation in the FeSNC/PMS system.

FeSNC may cooperate with PMS to form complex complexes Fe–OSO_4 or Fe–(OH)–OSO_3, followed by electron transfer and O–O bond cleavage to produce the high-valent iron–oxo complexes $Fe^{(M)}$=O (M = IV, V, and VI).[68] Ultimately, the generated $^1O_2$ and high-valent iron–oxo complexes degraded the electron-rich organic pollutants into small molecules, a portion of which were thoroughly mineralized to produce CO_2 and H_2O.

3.5 Environmental tolerance and sustainable water treatment

Various common inorganic anions in aqueous humor possibly affect the catalyst activation performance. To investigate the effect of the system on the degradation of BPA in the presence of different common anions, 20 mM Cl^-, NO_3^-, HCO_3^- and $H_2PO_3^-$ were added to the system, respectively. As can be seen from Fig. 7(a), when HCO_3^- and $H_2PO_3^-$ were added to the solution, the degradation rate of BPA reached 100% after 3–4 min, and the removal rate slightly decreased compared with that of the blank control group; when Cl^- and NO_3^- were added to the solution, the degradation rate of BPA reached 100% after about 2 min, which was consistent with that of the blank control group. The possible reasons for this are that HCO_3^- and $H_2PO_3^-$ in water compete with BPA to consume PMS or induce the generation of ROS with lower reaction rates.[69,70] Overall, it seems that the main reaction ROS generated by catalyst FeSNC in the FeSNC-PMS system is little disturbed by ionic changes in the water.

The mineralization capacity of the FeSNC-PMS system was evaluated by measuring the total carbon removal within 10 min by TOC meter. The results in Fig. 7(b) show that the mineralization rate of BPA rapidly decreases by about 15% within 1 min, and the mineralization rate of BPA can reach 22% at 10 min, indicating that although the FeSNC-PMS system can rapidly destroy the structure of BPA, only a part of BPA is mineralized in the overall reaction process. The reason may be that the mineralization ability of the high-valent iron oxide species as the main ROS is not as good as that of the $SO_4^{\cdot-}$ and $^{\cdot}OH$ radicals, which are selective oxidizers, which is in line with the results of previous studies.[69]

To identify the selectivity of the FeSNC-PMS system for the degradation of different types of refractory organics, different types of refractory organics (BPA, RhB, 4-CP, NB, SMX, TC, BA, 4-NP, and OFL) were selected for the catalytic degradation. The results in Fig. 7(c) show that the FeSNC-PMS system can effectively remove the dye (RhB), antibiotics (SMX, OFL, and TC), chlorinated phenolics (4-CP), and endocrine disruptors (BPA), but it is difficult to effectively degrade NB, BA, and 4-NP which suggests that the system has the selectivity of catalytic oxidative degradation of different types of pollutants. Among them, NB, BA, and 4-NP are electron-deficient organics, while dyes,

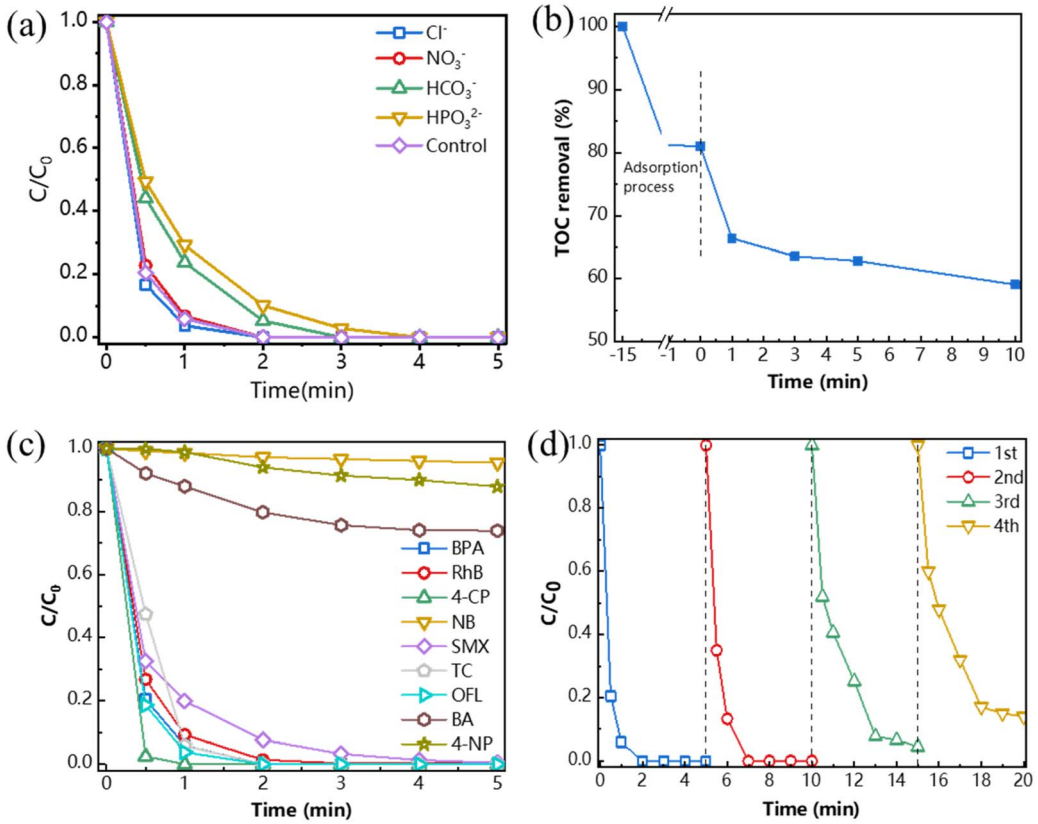

Fig. 7 (a) Kinetic curves of BPA degradation by FeSNC-PMS system in the presence of different coexisting anions; (b) TOC removal efficiency in FeSNC-PMS system. (c) Kinetic curves of FeSNC-PMS system for degradation of different organic pollutants; (d) cycling stability experiments of FeSNC-PMS system for BPA degradation.

antibiotics, chlorinated phenolics, and endocrine disruptors are electron-rich organics.[31,65,71] Electron-deficient organics are usually not easily degraded by the non-radical pathway, and their degradation mainly relies on oxidizing sulfate and hydroxyl radicals, whereas electron-rich pollutants, with electron-rich groups, are more biochemically reactive and can be degraded by the slightly less oxidizing non-radical pathway.[72]

Four cycle experiments were performed on FeSNC to evaluate the reusability and stability of FeSNC catalyst. In recovering the catalyst, it was washed in alcohol and water, then centrifuged and dried, and pyrolyzed at 900 °C for 3 h under the same conditions as for the preparation of the catalyst. The results of the tests are shown in Fig. 7(d), where the removal of BPA at 5 min for the four cycles was 100%, 100%, 95.5%, and 86.3%, respectively, and the corresponding apparent rate constant k_{obs} were 2.832 min^{-1}, 2.016 min^{-1}, 0.621 min^{-1}, and 0.548 min^{-1}, respectively. The apparent rate constant k_{obs} decreased significantly in the four cycles, and the system was unable to degrade BPA by 100% in the third cycle and thereafter, which may be due to the accumulation of intermediates or loss of metal active sites on the catalyst surface during the degradation process. In addition, the poor dispersion of the catalyst after the two reactions observed in the experiments may also be one of the key factors leading to the decrease in the ability to degrade BPA. The metal ions content in the reaction solution after the cycling experiment was detected by ICP-OES, and it was found that the iron ions were below the detection limit (0.02 mg L^{-1}), which was much lower than the 10 mg L^{-1} stipulated in the national emission standard GB31962-2015, and it would not cause the secondary pollution in the practical use. It indicates that FeSNC catalyst has certain reusability.

4 Conclusions

In this study, we have developed a highly dispersed Fe-based sulfur–nitrogen co-doped porous carbon catalyst (FeSNC), which exhibits unprecedented reaction rate and selectivity for activation of PMS and removal of bisphenol A from the water column. The FeSNC/PMS system was the most effective in the degradation of 20 mg L^{-1} of BPA with the FeSNC dosage of 0.1 g L^{-1} and the PMS concentration of 1 mM. The best effect was achieved with 100% degradation in 3 min and an apparent rate constant of 2.83 min^{-1}. The catalytic effect was quite stable in the range of pH 3–9, and was not affected by environmental factors such as ions in the water and quenching effect of organics, *etc.* The concentration of Fe ions dissolved was much lower than that of the environmental emission standard (<0.01 mg L^{-1}), and it had a certain degree of reusability. The intrinsic constitutive relationship between active species and pollutant removal was insightfully understood by combining experimental analyses with characterization techniques. Two non-radical degradation pathways, namely, the high-valent iron oxidation pathway and the singlet oxygen, were predominantly present in the FeSNC/PMS system, in which the main reactive oxygen species were high-valent iron-oxidizing species; and the FeSNC/PMS system was inclined to degrade the electron-rich organic pollutants with oxidative selectivity. This work provides potential guidance for synthesis strategies of efficient metal catalysts and PMS-based water purification processes.

Data availability

The data that support the findings of this study are available from the corresponding author upon reasonable request.

Author contributions

Yu Sun: conceptualization, methodology, formal analysis, investigation, writing – original draft, writing – review & editing. Chuning Zhang: methodology, formal analysis, investigation, data curation. Yan Jia: conceptualization, investigation, writing – original draft, supervision, writing – review & editing. Yalei Zhang: funding acquisition, resources, supervision. Jianwei Fan: funding acquisition, resources, supervision.

Conflicts of interest

There are no conflicts to declare.

Acknowledgements

This work was financially supported by the National Natural Science Foundation of China (52370044 and 52370085).

References

1 X. Ji, J. Liang, Y. Wang, X. Liu, Y. Li, Q. Liu, *et al.*, Synthetic Antioxidants as Contaminants of Emerging Concern in Indoor Environments: Knowns and Unknowns, *Environ. Sci. Technol.*, 2023, **57**(51), 21550–21557.
2 Z. Tian, K. T. Peter, A. D. Gipe, H. Zhao, F. Hou, D. A. Wark, *et al.*, Suspect and Nontarget Screening for Contaminants of Emerging Concern in an Urban Estuary, *Environ. Sci. Technol.*, 2020, **54**(2), 889–901.
3 D. Yadav, S. Rangabhashiyam, P. Verma, P. Singh, P. Devi, P. Kumar, *et al.*, Environmental and health impacts of contaminants of emerging concerns: Recent treatment challenges and approaches, *Chemosphere*, 2021, **272**, 129492.
4 T. Liu, S. Xiao, N. Li, J. Chen, X. Zhou, Y. Qian, *et al.*, Water decontamination via nonradical process by nanoconfined Fenton-like catalysts, *Nat. Commun.*, 2023, **14**(1), 2881.
5 G. P. Anipsitakis and D. D. Dionysiou, Degradation of organic contaminants in water with sulfate radicals generated by the conjunction of peroxymonosulfate with cobalt, *Environ. Sci. Technol.*, 2003, **37**(20), 4790–4797.
6 M. Kohantorabi, G. Moussavi and S. Giannakis, A review of the innovations in metal- and carbon-based catalysts explored for heterogeneous peroxymonosulfate (PMS) activation, with focus on radical vs . non-radical degradation pathways of organic contaminants, *Chem. Eng. J.*, 2021, **411**, 127957.
7 X. Li, Y. Jia, J. Zhang, Y. Qin, Y. Wu, M. Zhou, *et al.*, Efficient removal of tetracycline by H_2O_2 activated with iron-doped

biochar: Performance, mechanism, and degradation pathways, *Chin. Chem. Lett.*, 2022, **33**(4), 2105–2110.

8 Y. Chen, Y. Mu, L. Tian, L.-L. Zheng, Y. Mei, Q.-J. Xing, *et al.*, Targeted Decomplexation of Metal Complexes for Efficient Metal Recovery by Ozone/Percarbonate, *Environ. Sci. Technol.*, 2023, **57**(12), 5034–5045.

9 Q. Zeng, Y. Wen, X. Duan, X. Xu, J. Tan, Q. Zhang, *et al.*, Single-atom Ni-N4 sites coordinate dual nonradical oxidation pathways via peroxymonosulfate activation: Computational insights and in situ spectroscopic analyses, *Appl. Catal., B*, 2024, **346**, 123752.

10 C. Solís-Balbín, D. Sol, A. Laca, A. Laca and M. Díaz, Destruction and entrainment of microplastics in ozonation and wet oxidation processes, *J. Water Proc. Eng.*, 2023, **51**, 103456.

11 Y. Ding, L. Fu, X. Peng, M. Lei, C. Wang and J. Jiang, Copper catalysts for radical and nonradical persulfate based advanced oxidation processes: Certainties and uncertainties, *Chem. Eng. J.*, 2022, **427**, 131776.

12 Y. Gao, Y. Zhou, S.-Y. Pang, J. Jiang, Y.-M. Shen, Y. Song, *et al.*, Enhanced peroxymonosulfate activation via complexed Mn(II): A novel non-radical oxidation mechanism involving manganese intermediates, *Water Res.*, 2021, **193**, 116856.

13 L. H. Zhang, Y. Shi, Y. Wang and N. R. Shiju, Nanocarbon Catalysts: Recent Understanding Regarding the Active Sites, *Adv. Sci.*, 2020, **7**(5), 2070028.

14 X. Li, G. Zhang, Y. Jia, W. Zou, G. Zhang, Y. Pan, *et al.*, Removal of bisphenol A in a heterogeneous Fenton system via biochar synthesized using different Fe precursors: Properties, effects, and mechanisms, *Sci. Total Environ.*, 2024, **912**, 168855.

15 X. Li, G. Zhang, M. Zhang, Q. Cui, W. Zou and M. Zhou, Accelerated removal of organic pollutants by biochar-based iron carbon granule-activated periodate in chloride-containing water: The role of active chlorine, *Sep. Purif. Technol.*, 2024, **351**, 128029.

16 J. Liang, L. Fu, K. Gao and X. Duan, Accelerating radical generation from peroxymonosulfate by confined variable Co species toward ciprofloxacin mineralization: ROS quantification and mechanisms elucidation, *Appl. Catal., B*, 2022, **315**, 121542.

17 Y. Liu, L. Qiu, Q. Nan, J. Wang, J. R. Zhao, T. Li, *et al.*, One-pot synthesis of mesoporous silicas supported Cu single-atom and CuO nanoparticles for peroxymonosulfate-activated degradation of tetracycline over a wide pH range, *Microporous Mesoporous Mater.*, 2022, **333**, 111729.

18 Y. Jia, Y. Chen, Y. Xue and J. Fan, Efficient activation of peroxymonosulfate by Mn single-atom: Critical role of Mn-N4 coordination for generating singlet oxygen, *Sep. Purif. Technol.*, 2024, **335**, 126129.

19 J. Wang and S. Wang, Activation of persulfate (PS) and peroxymonosulfate (PMS) and application for the degradation of emerging contaminants, *Chem. Eng. J.*, 2018, **334**, 1502–1517.

20 W. Qu, M. Luo, Z. Tang, T. Zhong, H. Zhao, L. Hu, *et al.*, Accelerated Catalytic Ozonation in a Mesoporous Carbon-Supported Atomic Fe–N4 Sites Nanoreactor: Confinement Effect and Resistance to Poisoning, *Environ. Sci. Technol.*, 2023, **57**(35), 13205–13216.

21 L. Chen, S. Wang, Z. Yang, J. Qian and B. Pan, Selective interfacial oxidation of organic pollutants in Fenton-like system mediated by Fe(III)-adsorbed carbon nanotubes, *Appl. Catal., B*, 2021, **292**, 120193.

22 C. Cheng, W. Ren, F. Miao, X. Chen, X. Chen and H. Zhang, Generation of Fe^{IV}=O and its Contribution to Fenton-Like Reactions on a Single-Atom Iron-N-C Catalyst, *Angew. Chem., Int. Ed.*, 2023, **62**(10), e202218510.

23 A. Han, W. Sun, X. Wan, D. Cai, X. Wang, F. Li, *et al.*, Construction of Co_4 Atomic Clusters to Enable Fe-N_4 Motifs with Highly Active and Durable Oxygen Reduction Performance, *Angew. Chem., Int. Ed.*, 2023, **62**(30), e202303185.

24 D. Guo, R. Shibuya, C. Akiba, S. Saji, T. Kondo and J. Nakamura, Active sites of nitrogen-doped carbon materials for oxygen reduction reaction clarified using model catalysts, *Science*, 2016, **351**(6271), 361–365.

25 D. Usachov, O. Vilkov, A. Grüneis, D. Haberer, A. Fedorov, V. K. Adamchuk, *et al.*, Nitrogen-doped graphene: Efficient growth, structure, and electronic properties, *Nano Lett.*, 2011, **11**(12), 5401–5407.

26 B. Li, Q. Li and X. Wang, Iron/iron carbide coupled with S, N co-doped porous carbon as effective oxygen reduction reaction catalyst for microbial fuel cells, *Environ. Res.*, 2023, **228**, 115808.

27 L. Jiao, Y. Kang, Y. Chen, N. Wu, Y. Wu, W. Xu, *et al.*, Unsymmetrically coordinated single Fe-N3S1 sites mimic the function of peroxidase, *Nano Today*, 2021, **40**, 101261.

28 H. Liu, L. Jiang, Y. Sun, J. Khan, B. Feng, J. Xiao, *et al.*, Revisiting the Role of Sulfur Functionality in Regulating the Electron Distribution of Single-Atomic Fe Sites Toward Enhanced Oxygen Reduction, *Adv. Funct. Mater.*, 2023, **33**(35), 2304074.

29 Y. Li, H. Zhang, Y. Wang, P. Liu, H. Yang, X. Yao, *et al.*, A self-sponsored doping approach for controllable synthesis of S and N co-doped trimodal-porous structured graphitic carbon electrocatalysts, *Energy Environ. Sci.*, 2014, **7**(11), 3720–3726.

30 N. Jiang, H. Xu, L. Wang, J. Jiang and T. Zhang, Nonradical Oxidation of Pollutants with Single-Atom-Fe(III)-Activated Persulfate: Fe(V) Being the Possible Intermediate Oxidant, *Environ. Sci. Technol.*, 2020, **54**(21), 14057–14065.

31 X. Mi, P. Wang, S. Xu, L. Su, H. Zhong, H. Wang, *et al.*, Almost 100 % Peroxymonosulfate Conversion to Singlet Oxygen on Single-Atom CoN_{2+2} Sites, *Angew. Chem., Int. Ed.*, 2021, **60**(9), 4588–4593.

32 M. W. Smith, I. Dallmeyer, T. J. Johnson, C. S. Brauer, J.-S. McEwen, J. F. Espinal, *et al.*, Structural analysis of char by Raman spectroscopy: Improving band assignments through computational calculations from first principles, *Carbon*, 2016, **100**, 678–692.

33 K. Pang, W. Sun, F. Ye, L. Yang, M. Pu, C. Yang, *et al.*, Sulfur-modified chitosan derived N,S-co-doped carbon as a bifunctional material for adsorption and catalytic

degradation sulfamethoxazole by persulfate, *J. Hazard. Mater.*, 2022, **424**, 127270.

34 Y. Jiang, J. Wang, B. Liu, W. Jiang, T. Zhou, Y. Ma, *et al.*, Superhydrophilic N,S,O-doped Co/CoO/Co9S8@carbon derived from metal-organic framework for activating peroxymonosulfate to degrade sulfamethoxazole: Performance, mechanism insight and large-scale application, *Chem. Eng. J.*, 2022, **446**, 137361.

35 Y. Zhou, J. Jiang, Y. Gao, J. Ma, S.-Y. Pang, J. Li, *et al.*, Activation of Peroxymonosulfate by Benzoquinone: A Novel Nonradical Oxidation Process, *Environ. Sci. Technol.*, 2015, **49**(21), 12941–12950.

36 Y. Gao, Y. Zhu, T. Li, Z. Chen, Q. Jiang, Z. Zhao, *et al.*, Unraveling the High-Activity Origin of Single-Atom Iron Catalysts for Organic Pollutant Oxidation via Peroxymonosulfate Activation, *Environ. Sci. Technol.*, 2021, **55**(12), 8318–8328.

37 Q. Feng, J. Zhou, W. Luo, L. Ding and W. Cai, Photo-Fenton removal of tetracycline hydrochloride using $LaFeO_3$ as a persulfate activator under visible light, *Ecotoxicol. Environ. Saf.*, 2020, **198**, 110661.

38 Z. Guan, X. Zhang, W. Chen, J. Pei, D. Liu, Y. Xue, *et al.*, Mesoporous S doped Fe-N-C materials as highly active oxygen reduction reaction catalyst, *Chem. Commun.*, 2018, **54**(85), 12073–12076.

39 Y. Mun, S. Lee, K. Kim, S. Kim, S. Lee, J. W. Han, *et al.*, Versatile Strategy for Tuning ORR Activity of a Single Fe-N_4 Site by Controlling Electron-Withdrawing/Donating Properties of a Carbon Plane, *J. Am. Chem. Soc.*, 2019, **141**(15), 6254–6262.

40 C. Chu, J. Yang, X. Zhou, D. Huang, H. Qi, S. Weon, *et al.*, Cobalt Single Atoms on Tetrapyridomacrocyclic Support for Efficient Peroxymonosulfate Activation, *Environ. Sci. Technol.*, 2021, **55**(2), 1242–1250.

41 A. Rastogi, S. R. Ai-Abed and D. D. Dionysiou, Sulfate radical-based ferrous-peroxymonosulfate oxidative system for PCBs degradation in aqueous and sediment systems, *Appl. Catal., B*, 2009, **85**(3–4), 171–179.

42 Y. Duan, Y. Liu, Y. Wang, H. Wang, W. Yin and G. Xu, Recyclable Fe/S co-doped nanocarbon derived from metal-organic framework as a peroxymonosulfate activator for efficient removal of 2,4-dichlorophenol, *Environ. Sci. Pollut. Res.*, 2023, **30**(3), 6906–6918.

43 M. F. Gasim, A. Veksha, G. Lisak, S.-C. Low, T. S. Hamidon, M. H. Hussin, *et al.*, Importance of carbon structure for nitrogen and sulfur co-doping to promote superior ciprofloxacin removal via peroxymonosulfate activation, *J. Colloid Interface Sci.*, 2023, **634**, 586–600.

44 X. Li, Y. Jia, M. Zhou, X. Su and J. Sun, High-efficiency degradation of organic pollutants with Fe, N co-doped biochar catalysts via persulfate activation, *J. Hazard. Mater.*, 2020, **397**, 122764.

45 S. Waclawek, H. V. Lutze, K. Grubel, V. V. T. Padil, M. Cernik and D. D. Dionysiou, Chemistry of persulfates in water and wastewater treatment: A review, *Chem. Eng. J.*, 2017, **330**, 44–62.

46 K. Govindan, M. Raja, M. Noel and E. J. James, Degradation of pentachlorophenol by hydroxyl radicals and sulfate radicals using electrochemical activation of peroxomonosulfate, peroxodisulfate and hydrogen peroxide, *J. Hazard. Mater.*, 2014, **272**, 42–51.

47 J. He, Y. Wan and W. Zhou, ZIF-8 derived Fe-N coordination moieties anchored carbon nanocubes for efficient peroxymonosulfate activation via non-radical pathways: Role of FeN_x sites, *J. Hazard. Mater.*, 2021, **405**, 124199.

48 X. Peng, J. Wu, Z. Zhao, X. Wang, H. Dai, L. Xu, *et al.*, Activation of peroxymonosulfate by single-atom Fe-g-C3N4 catalysts for high efficiency degradation of tetracycline via nonradical pathways: Role of high-valent iron-oxo species and Fe-Nx sites, *Chem. Eng. J.*, 2022, **427**, 130803.

49 Y. Ding, X. Wang, L. Fu, X. Peng, C. Pan, Q. Mao, *et al.*, Nonradicals induced degradation of organic pollutants by peroxydisulfate (PDS) and peroxymonosulfate (PMS): Recent advances and perspective, *Sci. Total Environ.*, 2021, **765**, 142794.

50 H. Jin, S. Sultan, M. Ha, J. N. Tiwari, M. G. Kim and K. S. Kim, Simple and Scalable Mechanochemical Synthesis of Noble Metal Catalysts with Single Atoms toward Highly Efficient Hydrogen Evolution, *Adv. Funct. Mater.*, 2020, **30**(25), 2000531.

51 Z. Li, Y. Huo, T. Li, S. Dong, M. Huo, G. Liu, *et al.*, Toward Practical Water Decontaminations via Peroxymonosulfate Nonradical Oxidation: The Role of Cocatalyst MoS2 with Sulfur Vacancies, *ACS ES&T Eng.*, 2023, **3**(11), 1975–1985.

52 S.-S. Liu, H. Fu, F. Wang, Y. Wei, B. Meng, P. Wang, *et al.*, Insight into the extremely different catalytic behaviors of asymmetric and symmetric oxygen vacancies for peroxymonosulfate activation, *Appl. Catal., B*, 2024, **346**, 123753.

53 Y. Jia, Y. Chen, Y. Xue and J. Fan, Efficient activation of peroxymonosulfate by Mn single-atom: Critical role of Mn-N4 coordination for generating singlet oxygen, *Sep. Purif. Technol.*, 2024, **335**, 126129.

54 Z. Guan, Y. Zhang, S. Zuo, S. Zhu, W. Wang and D. Li, The synergistic catalytic mechanism between different functional sites of boron/iron on iron oxides in Fenton-like reactions, *Sep. Purif. Technol.*, 2023, **312**, 123391.

55 L. Zhang, J. Qi, W. Chen, X. Yang, Z. Fang, J. Li, *et al.*, Constructing Hollow Multishelled Microreactors with a Nanoconfined Microenvironment for Ofloxacin Degradation through Peroxymonosulfate Activation: Evolution of High-Valence Cobalt-Oxo Species, *Environ. Sci. Technol.*, 2023, **57**(42), 16141–16151.

56 X. Hu and M. Zhu, Were Persulfate-Based Advanced Oxidation Processes Really Understood? Basic Concepts, Cognitive Biases, and Experimental Details, *Environ. Sci. Technol.*, 2024, **58**(24), 10415–10444.

57 X. Cheng, W. Zhou, P. Li, Z. Ren, D. Wu, C. Luo, *et al.*, Improving ultrafiltration membrane performance with pre-deposited carbon nanotubes/nanofibers layers for drinking water treatment, *Chemosphere*, 2019, **234**, 545–557.

58 P. Sun, H. Liu, M. Feng, L. Guo, Z. Zhai, Y. Fang, *et al.*, Nitrogen-sulfur co-doped industrial graphene as an

efficient peroxymonosulfate activator: Singlet oxygen-dominated catalytic degradation of organic contaminants, *Appl. Catal., B*, 2019, **251**, 335–345.

59 Y. Li, T. Yang, S. Qiu, W. Lin, J. Yan, S. Fan, *et al.*, Uniform N-coordinated single-atomic iron sites dispersed in porous carbon framework to activate PMS for efficient BPA degradation via high-valent iron-oxo species, *Chem. Eng. J.*, 2020, **389**, 124382.

60 Y. Zhu, Z. Quan, B. Zhang, J. Zheng, J. Wang, X. Zhang, *et al.*, Enhanced performance of carbon dots and Mn3O4 composite by phosphate in peroxymonosulfate activation, *Appl. Catal., B*, 2024, **351**, 123954.

61 L. Wu, Z. Sun, Y. Zhen, S. Zhu, C. Yang, J. Lu, *et al.*, Oxygen Vacancy-Induced Nonradical Degradation of Organics: Critical Trigger of Oxygen (O2) in the Fe–Co LDH/Peroxymonosulfate System, *Environ. Sci. Technol.*, 2021, **55**(22), 15400–15411.

62 Y. Si, Z.-Y. Guo, Y. Meng, H.-H. Li, L. Chen, A.-Y. Zhang, *et al.*, Reusing Sulfur-Poisoned Palladium Waste as a Highly Active, Nonradical Fenton-like Catalyst for Selective Degradation of Phenolic Pollutants, *Environ. Sci. Technol.*, 2022, **56**(1), 564–574.

63 M. Li, H. Li, C. Ling, H. Shang, H. Wang, S. Zhao, *et al.*, Highly selective synthesis of surface FeIV=O with nanoscale zero-valent iron and chlorite for efficient oxygen transfer reactions, *Proc. Natl. Acad. Sci. U. S. A.*, 2023, **120**(38), e2304562120.

64 Y. Lei, Y. Yu, X. Lei, X. Liang, S. Cheng, G. Ouyang, *et al.*, Assessing the Use of Probes and Quenchers for Understanding the Reactive Species in Advanced Oxidation Processes, *Environ. Sci. Technol.*, 2023, **57**(13), 5433–5444.

65 Y. Qi, J. Li, Y. Zhang, Q. Cao, Y. Si, Z. Wu, *et al.*, Novel lignin-based single atom catalysts as peroxymonosulfate activator for pollutants degradation: Role of single cobalt and electron transfer pathway, *Appl. Catal., B*, 2021, **286**, 119910.

66 Y. Gao, T. Wu, C. Yang, C. Ma, Z. Zhao, Z. Wu, *et al.*, Activity Trends and Mechanisms in Peroxymonosulfate-Assisted Catalytic Production of Singlet Oxygen over Atomic Metal-N-C Catalysts, *Angew. Chem., Int. Ed.*, 2021, **60**(41), 22513–22521.

67 X. Li, X. Huang, S. Xi, S. Miao, J. Ding, W. Cai, *et al.*, Single Cobalt Atoms Anchored on Porous N-Doped Graphene with Dual Reaction Sites for Efficient Fenton-like Catalysis, *J. Am. Chem. Soc.*, 2018, **140**(39), 12469–12475.

68 Y. Bao, C. Lian, K. Huang, H. Yu, W. Liu, J. Zhang, *et al.*, Generating High-valent Iron-oxo $\equiv Fe^{IV}=O$ Complexes in Neutral Microenvironments through Peroxymonosulfate Activation by Zn-Fe Layered Double Hydroxides, *Angew. Chem., Int. Ed.*, 2022, **61**(42), e202209542.

69 J. Lee, U. von Gunten and J.-H. Kim, Persulfate-Based Advanced Oxidation: Critical Assessment of Opportunities and Roadblocks, *Environ. Sci. Technol.*, 2020, **54**(6), 3064–3081.

70 S. Chen, M. Cai, Y. Liu, L. Zhang and L. Feng, Effects of water matrices on the degradation of naproxen by reactive radicals in the UV/peracetic acid process, *Water Res.*, 2019, **150**, 153–161.

71 H. Lu, M. Sui, B. Yuan, J. Wang and Y. Lv, Efficient degradation of nitrobenzene by Cu-Co-Fe-LDH catalyzed peroxymonosulfate to produce hydroxyl radicals, *Chem. Eng. J.*, 2019, **357**, 140–149.

72 S. Giannakis, K.-Y. A. Lin and F. Ghanbari, A review of the recent advances on the treatment of industrial wastewaters by Sulfate Radical-based Advanced Oxidation Processes (SR-AOPs), *Chem. Eng. J.*, 2021, **406**, 127083.